Frequency-dependent fundamental and dipole gap solitons in $\mathcal{PT}$-symmetric nonlinear metamaterials

Juan Bai,[1] Xiaoqin Bai,[1] Zhipei Gao,[1] and Rongcao Yang[1,2,*]

[1]*School of Physics and Electronics Engineering, Shanxi University, Taiyuan 030006, China*

[2]*Collaborative Innovation Center of Extreme Optics, Shanxi University, Taiyuan 030006, China*

(Received 13 January 2024; accepted 2 April 2024; published 18 April 2024)

We derive a theoretical model with frequency-dependent parameters for describing the transmission of electromagnetic waves in $\mathcal{PT}$-symmetric metamaterials (MMs). Based on the derived theoretical model, we investigate the tunable band structure and eigenvalue problem in the negative or positive index region of MMs, and predict the existence and stability of fundamental, out-of-phase, and in-phase dipole gap solitons in defocusing or focusing nonlinear $\mathcal{PT}$-symmetric MMs. Furthermore, we discuss the enhanced localization of solitons under different formation conditions. The results reveal that there exist abundant gap solitons with frequency controllability in $\mathcal{PT}$-symmetric MMs, and the established theoretical model paves the way to explore more solitons in $\mathcal{PT}$-symmetric MMs.

DOI: 10.1103/PhysRevA.109.043518

I. INTRODUCTION

It has been demonstrated that in quantum mechanics, a non-Hermitian Hamiltonian obeying parity-time ($\mathcal{PT}$) symmetry may possess fully real eigenvalue spectra [1–3]. Bender and colleagues pointed out that a non-Hermitian Hamiltonian $\hat{H} = -\partial_x^2 + V(x)$ with a $\mathcal{PT}$-symmetric potential $V(x)$ commutes with the $\mathcal{PT}$ operator $\hat{P}\hat{T}$, i.e., $[\hat{H}, \hat{P}\hat{T}] = 0$, implying that $\hat{H}$ and $\hat{P}\hat{T}$ share the common eigenfunctions and skewed vector space of the eigenmodes [1,2]. A necessary but insufficient condition for a Hamiltonian to be $\mathcal{PT}$ symmetric is $V(x) = V^*(-x)$, leading to a potential with even real and odd imaginary parts. In recent years, $\mathcal{PT}$ symmetry has been widely applied in atom and quantum mechanics [4,5], acoustics [6,7], mechanics [8], electrical circuits [9], and nonlinear optics [10,11]. Drawing an analogy between the paraxial approximation equation for optical beams propagation and the Schrödinger equation in quantum mechanics [12,13], $\mathcal{PT}$-symmetric potentials in optical systems can be characterized by the complex refractive index $n(x) = n_R(x) + in_I(x)$, which can be physically realized by involving symmetric index guiding $n_R(-x) = n_R(x)$ and antisymmetric gain-loss $n_I(-x) = -n_I(x)$ [14]. On the basis of the judicious design of the complex refractive index, various $\mathcal{PT}$-symmetric optical systems including $\mathcal{PT}$-symmetric couplers [15,16] and photonic lattices [13,17] have been proposed. Novel characteristics of $\mathcal{PT}$ symmetry were observed, such as power oscillation [14], and loss induced transparency and spontaneous $\mathcal{PT}$ symmetry breaking [18,19]. Recently, the $\mathcal{PT}$ symmetry has been extended to the nonlinear physical systems, and $\mathcal{PT}$-symmetric solitons governed by the nonlinear Schrödinger equation (NLSE) have been extensively investigated [20–29]. The solitons and their stability in $\mathcal{PT}$-symmetric optical lattices [20,21] and generalized Scarf-II potential [22] were reported. Double-hump solitons were studied with the $\mathcal{PT}$-symmetric harmonic-hyperbolic-Gaussian potentials [23] and Dirac-$\delta(x)$-Scarf-II potentials [24]. Dark solitons and vortices [25] as well as the symmetry breaking of $\mathcal{PT}$-symmetric solitons [26,27] were investigated. The switching dynamics of a bistable soliton in a $\mathcal{PT}$-symmetric fiber coupler [28] and a single gap soliton and soliton clusters in saturable nonlinear media [29] were also reported.

On the other hand, metamaterials (MMs), consisting of periodically arranged metal-dielectric units, have attracted much attention due to their unique characteristics, such as negative refraction [30], and strong dispersion and adjustable electromagnetic (EM) response [31]. However, MMs with metal-dielectric structures have unavoidable material loss, which is unfavorable in physical application except for energy absorption. Many efforts including low-loss material employment and gain compensation [32,33] have been used to overcome the loss of MMs, or to exploit loss in $\mathcal{PT}$-symmetric MMs [32–37], such as matching the permittivity or/and the permeability [34], featuring a negative-resistance device [35], and providing negative surface conductance graphene metasurface [36]. Lazarides and Tsironis first proposed a one-dimensional (1D) $\mathcal{PT}$-symmetric magnetic MM consisting of split-ring dimers with balanced gain and loss [37]. Sun *et al.* constructed a $\mathcal{PT}$ symmetry coupled-resonators system by balancing the scattering and dissipative loss in experiments [38]. Alaeian and Dionne reported a five-layer "metal-insulator-metal" $\mathcal{PT}$-symmetric plasmonic MM [39]. Gear *et al.* constructed a 1D photonic crystal through alternating dielectric slabs with loss and magnetic slabs with gain [34]. $\mathcal{PT}$-symmetric MMs are of great interest in manipulating EM waves by engineering the complex refractive index in dielectric permittivity and the magnetic permeability plane, which brings about many important physical phenomena. Recently, several works focusing on beam transmission

*sxdxyrc@sxu.edu.cn

in $\mathcal{PT}$-symmetric epsilon-near-zero MMs have been reported [40,41]. For example, Savoia *et al.* studied the $\mathcal{PT}$-symmetry-induced exponentially bound modes at the interface between two media [40], Nicolussi *et al.* analyzed the asymmetric reflection and the enhanced transmission based on the transmission line theory [41]. Moreover, the transmission of EM waves in non-$\mathcal{PT}$-symmetric MMs has also received much attention [42–47]. Scalora *et al.* derived a general NLSE to describe the propagation of ultrashort pulses in nonlinear MMs [42]. Lazarides and Tsironis [43] and Wen *et al.* [45] successively reported coupled theoretical models in MMs and revealed the role of the dispersive electric permittivity and magnetic permeability. Li *et al.* analytically investigated three types of gray solitons in MMs based on a derived higher-order model [46]. Zhu and Chen studied the modulation of periodic waves and solitons in MMs with high-order effects [47]. Shafeeque Ali *et al.* discovered the formation of three-dimensional (3D) light bullets in MMs with the balance between the dispersion and nonlinearity effects [48]. To reveal the transmission characteristics of EM waves in $\mathcal{PT}$-symmetric MMs, it is imperative to establish a theoretical model for describing the transmission of EM waves in $\mathcal{PT}$-symmetric MMs. Moreover, in view of the unique controllable frequency-dependent EM properties of MMs, it is also important to explore the existence and controllable transmission of the solitons in $\mathcal{PT}$-symmetric MMs.

In this work, motivated by the works of solitons in $\mathcal{PT}$-symmetric optical lattices mentioned above, we firstly derive a theoretical model to describe the EM waves transmission in $\mathcal{PT}$-symmetric MMs. Based on the derived transmission model and the tunable dispersion characteristics of $\mathcal{PT}$-symmetric MMs, we study the frequency-dependent band structure and eigenvalue problem, and predict the existence, stability, and controllability of fundamental, out-of-phase dipole (out-dipole) and in-phase dipole (in-dipole) solitons in the negative or positive index region of defocusing or focusing nonlinear $\mathcal{PT}$-symmetric MMs. Furthermore, the stability of these solitons is verified by direct simulations, and their enhanced localizations are discussed in detail.

The remaining contents of this work are arranged as follows: In Sec. II, the nonlinear theoretical model describing the transmission of EM waves in $\mathcal{PT}$-symmetric MMs is derived, and the tunable parameters of the $\mathcal{PT}$-symmetric MMs are discussed. In Sec. III, the tunable band structure and the existence, stability, nonlinear dynamics, and localization of fundamental, out-dipole and in-dipole solitons in the negative or positive index region of $\mathcal{PT}$-symmetric nonlinear MMs are investigated in detail. Finally, the conclusion and discussion are presented in Sec. IV.

II. THEORETICAL MODEL AND PARAMETER ANALYSIS

It is well known that the transmission of the EM waves follows the Maxwell equations in both conventional materials and MMs: $\nabla \times \mathbf{E} = -\partial \mathbf{B}/\partial t$, $\nabla \times \mathbf{H} = \partial \mathbf{D}/\partial t$, $\nabla \cdot \mathbf{D} = 0$, $\nabla \cdot \mathbf{B} = 0$, where $\mathbf{E}$, $\mathbf{H}$, $\mathbf{D}$, and $\mathbf{B}$ are, respectively, electric field, magnetic field, and electric and magnetic flux densities obeying the constitutive relations $\mathbf{D} = \varepsilon\mathbf{E} + \mathbf{P}_{\rm NL}$ and $\mathbf{B} = \mu\mathbf{H} + \mu_0\mathbf{M}_{\rm NL}$ [45,46], where $\varepsilon = \varepsilon_0\varepsilon_r$ and $\mu = \mu_0\mu_r$ are the permittivity and permeability in vacuum with $\varepsilon_0\mu_0 = 1/c^2$, $\varepsilon_{\rm r}$ and $\mu_{\rm r}$ are the relative permittivity and relative permeability; $\mathbf{P}_{\rm NL} = \varepsilon_0\chi_{\rm p}|E_x|^2E_x$ and $\mathbf{M}_{\rm NL} = \chi_{\rm m}|H_y|^2H_y$ represent the nonlinear polarization and magnetization, respectively. Assuming the beam is operating at frequency ω_0 with the electric field $\mathbf{E} = \frac{1}{2}(\tilde{\mathbf{E}}e^{-i\omega_0 t} + \tilde{\mathbf{E}}^* e^{i\omega_0 t})$ and magnetic field $\mathrm{H} = \frac{1}{2}(\tilde{\mathrm{H}}e^{-i\omega_0 t} + \tilde{\mathrm{H}}^* e^{i\omega_0 t})$, and substituting them into the Maxwell equations, we can obtain the wave equations in the frequency domain as follows:

$$\nabla^2\tilde{\mathrm{E}} + \frac{\omega_0^2}{c^2}\varepsilon_{\rm r}\mu_{\rm r}\tilde{\mathrm{E}} + \frac{\omega_0^2}{c^2}\mu_{\rm r}\frac{\tilde{\mathrm{P}}_{NL}}{\varepsilon_0} + i\omega_0\mu_0\nabla\times\tilde{\mathrm{M}}_{NL} = 0, \quad (1a)$$

$$\nabla^2\tilde{\mathrm{H}} + \frac{\omega_0^2}{c^2}\varepsilon_{\rm r}\mu_{\rm r}\tilde{\mathrm{H}} + \frac{\omega_0^2}{c^2}\varepsilon_{\rm r}\tilde{\mathrm{M}}_{NL} + i\omega_0\nabla\times\tilde{\mathrm{P}}_{\rm NL} = 0, \quad (1b)$$

where the variables with tildes correspond to the Fourier transforms. For the TE mode propagating along the z axis, $\mathbf{E} = (E_x, 0, 0)$ and $\mathrm{H} = (0, H_y, 0)$ can be defined as [49]

$$E_x = A(y)\left[\int E(k_x, z)e^{-ik_x z}dk_x\right]e^{-ik_{z0}z}, \quad (2a)$$

$$H_y = A(y)\left[\int H(k_x, z)e^{-ik_x z}dk_x\right]e^{-ik_{z0}z}, \quad (2b)$$

where the integration defines a packet of waves with transverse wave number k_x and longitudinal wave number k_{z0} along the z axis. Here $E(k_x, z)$ and $H(k_x, z)$ are Fourier components related to z, and $A(y)$ is independent of z and satisfies the modal field equation. Substituting Eqs. (2a) and (2b) into Eqs. (1a) and (1b) and applying the method of separation of variables, one can obtain the equations for the electric field (similar forms for the magnetic field):

$$\frac{\partial^2 A}{\partial y^2} + \frac{\omega_0^2}{c^2}\mu_{\rm r}\Delta\varepsilon A = A\tilde{k}^2, \quad (3a)$$

$$2ik_{z0}\frac{\partial E}{\partial z} + \frac{\partial^2 E}{\partial z^2} - k_{z0}^2E - k_x^2E + \frac{\omega_0^2}{c^2}\varepsilon_{\rm r}\mu_{\rm r}E + \frac{\omega_0^2}{c^2}\varepsilon_{\rm r}\Delta\mu E = -E\tilde{k}^2, \quad (3b)$$

where $\tilde{k}^2 = k_z^2 + k_x^2 + \omega_0^2\Delta_{NL}/c^2$ is introduced to describe the nonlinear eigenvalue shift Δ_{NL} from the linear value [49]; ${k_x}^2$ and $\omega_0^2\Delta_{NL}/c^2$ can be viewed as a perturbation of ${k_z}^2$. After substituting $\tilde{k}^2$ into Eq. (3b) and combining the corresponding equations of the magnetic field, we can obtain the following coupled equations:

$$\frac{\partial^2 E_x}{\partial z^2} + 2ik_{z0}\frac{\partial E_x}{\partial z} + \left(k_z^2 - k_{z0}^2\right)E_x + \frac{\omega_0^2}{c^2}\varepsilon_{\rm r}\mu_{\rm r}E_x + \frac{\omega_0^2}{c^2}\varepsilon_{\rm r}\Delta\mu E_x + \frac{\omega_0^2}{c^2}\Delta_{NL}E_x = 0, \quad (4a)$$

$$\frac{\partial^2 H_y}{\partial z^2} + 2ik_{z0}\frac{\partial H_y}{\partial z} + \left(k_z^2 - k_{z0}^2\right)H_y + \frac{\omega_0^2}{c^2}\varepsilon_{\rm r}\mu_{\rm r}H_y + \frac{\omega_0^2}{c^2}\mu_{\rm r}\Delta\varepsilon H_y + \frac{\omega_0^2}{c^2}\Delta_{NL}H_y = 0. \quad (4b)$$

Here $\Delta_{NL} = \mu_r\Delta\varepsilon = \varepsilon_r\Delta\mu$ with $\Delta\varepsilon = \chi_p|E_x|^2$, $\Delta\mu = \chi_m|H_y|^2$, which can be derived from Eq. (3a) and its magnetic field counterpart by multiplying the complex amplitude A^* and integrating with respect to y [49]. Δ_{NL} represents but is not limited to the third-order nonlinearity. In Eqs. (4a)

and (4b), as k_z is approximately k_{z0} and $k_z^2 + k_x^2 = \text{const}$, $(k_z^2 - k_{z0}^2) \approx 2k_{z0}(k_z - k_{z0})$ and $k_z - k_{z0}$ can be expressed as a Taylor series in k_x with zero odd-order terms, i.e., $(\frac{\partial k_z}{\partial k_x})_{k_x=0} = (\frac{\partial^3 k_z}{\partial k_x^3})_{k_x=0} = 0$, and then only even-order derivative terms are included [49], i.e.,

$$k_z - k_{z0} \approx \frac{1}{2}\left(\frac{\partial^2 k_z}{\partial k_x^2}\right)_{k_x=0} k_x^2 + \frac{1}{24}\left(\frac{\partial^4 k_z}{\partial k_x^4}\right)_{k_x=0} {k_x}^4 + \cdots . \tag{5}$$

Performing the inverse Fourier transform of the second and fourth terms into x derivatives $-k_x^2 \to \frac{\partial^2}{\partial x^2}$, $-k_x^4 \to \frac{\partial^4}{\partial x^4}$, Eqs. (4a) and (4b) can be written as

$$\frac{\partial^2 E_x}{\partial z^2} + 2ik_{z0}\frac{\partial E_x}{\partial z} + \frac{\partial^2 E_x}{\partial x^2} - \frac{1}{4k_{z0}}\frac{\partial^4 E_x}{\partial x^4} + \frac{\omega_0^2}{c^2}\varepsilon_r\mu_r E_x + \frac{\omega_0^2}{c^2}(\mu_r\chi_{\rm p}|E_x|^2 + \varepsilon_{\rm r}\chi_{\rm m}|H_y|^2)E_x = 0, \tag{6a}$$

$$\frac{\partial^2 H_y}{\partial z^2} + 2ik_{z0}\frac{\partial H_y}{\partial z} + \frac{\partial^2 H_y}{\partial x^2} - \frac{1}{4k_{z0}}\frac{\partial^4 H_y}{\partial x^4} + \frac{\omega_0^2}{c^2}\varepsilon_r\mu_r H_y + \frac{\omega_0^2}{c^2}(\mu_r\chi_p|E_x|^2 + \varepsilon_r\chi_m|H_y|^2)H_y = 0. \tag{6b}$$

With the aid of the intrinsic relationship $|H_y/E_x|^2 = \varepsilon_0|\varepsilon_r/\mu_r|/\mu_0$, Eqs. (6a) and (6b) can be decoupled to one equation as follows:

$$\frac{\partial E_x}{\partial z} = \frac{i}{2nk_0}\frac{\partial^2 E_x}{\partial x^2} - \frac{i}{8(nk_0)^3}\frac{\partial^4 E_x}{\partial x^4} + \frac{ik_0}{2n}\varepsilon_r\mu_r E_x + \frac{ik_0}{2n}\mu_r\chi_p|E_x|^2E_x + \frac{ik_0}{2n}\varepsilon_r\chi_m\frac{\varepsilon_0}{\mu_0}\left|\frac{\varepsilon_r}{\mu_r}\right||E_x|^2E_x. \tag{7}$$

In general, for lossy MMs, the permittivity and permeability are complex, i.e., $\varepsilon = \varepsilon_0\varepsilon_r = \varepsilon_0(\varepsilon_{\rm rr} + i\varepsilon_{\rm ri})$ and $\mu = \mu_0\mu_r = \mu_0(\mu_{\rm rr} + i\mu_{\rm ri})$ [50], where $\varepsilon_{\rm rr}$, $\varepsilon_{\rm ri}$, $\mu_{\rm rr}$, and $\mu_{\rm ri}$ are, respectively, the real parts and imaginary parts of ε_r and μ_r in MMs. Equation (7) can be rewritten as

$$\frac{\partial E_x}{\partial z} = \frac{i}{2nk_0}\frac{\partial^2 E_x}{\partial x^2} - \frac{i}{8(nk_0)^3}\frac{\partial^4 E_x}{\partial x^4} + \frac{i}{2}k_0(n + i2\alpha)E_x + \frac{i}{2n}k_0\left[(\mu_{\rm rr} + i\mu_{\rm ri})\chi_{\rm p} + (\varepsilon_{\rm rr} + i\varepsilon_{\rm ri})\chi_{\rm m}\frac{\varepsilon_0}{\mu_0}\left|\frac{\varepsilon_{\rm rr}}{\mu_{\rm rr}}\right|\right] \times |E_x|^2E_x, \tag{8}$$

where $n = \pm\sqrt{\varepsilon_{\rm rr}\mu_{\rm rr}}$ and $\alpha = n(\bar{\varepsilon} + \bar{\mu})/2$ are the real and imaginary parts of the equivalent complex refractive index $n_{\rm eff} = n + i\alpha$, with $\bar{\varepsilon} = \varepsilon_{\rm ri}/\varepsilon_{\rm rr}$ and $\bar{\mu} = \mu_{\rm ri}/\mu_{\rm rr}$, respectively. On the right-hand side of Eq. (8), the first and second terms describe the second-order diffraction (SOD) and fourth-order diffraction (FOD), the third term is a linear potential related to the refractive index n and linear loss or gain α, and the last one represents the nonlinear effects, where $\eta_r = \eta_0\eta_{\rm rr}$ with $\eta_{\rm rr} = \sqrt{\mu_{\rm rr}/\varepsilon_{\rm rr}}$ is the parameter of material impedance. The parameters of the MMs can be described by the Drude model [46], $\varepsilon_{\rm rr}(\varpi) = 1 - \frac{1}{\varpi^2 + \tilde{\gamma}_{\rm e}^2}$, $\varepsilon_{\rm ri}(\varpi) = \frac{\tilde{\gamma}_{\rm e}}{\varpi(\varpi^2 + \tilde{\gamma}_{\rm e}^2)}$, $\mu_{\rm rr}(\varpi) = 1 - \frac{\varpi_{\rm p}^2}{(\varpi^2 + \tilde{\gamma}_{\rm m}^2)}$, and $\mu_{\rm ri}(\varpi) = \frac{\tilde{\gamma}_m\varpi_{\rm p}^2}{\varpi(\varpi^2 + \tilde{\gamma}_{\rm m}^2)}$, where $\varpi = \omega/\omega_{\rm pe}$, $\varpi_{\rm p} = \omega_{\rm pm}/\omega_{\rm pe}$, $\tilde{\gamma}_{\rm e} = \gamma_{\rm e}/\omega_{\rm pe}$, and $\tilde{\gamma}_{\rm m} = \gamma_{\rm m}/\omega_{\rm pe}$. Here $\omega_{\rm pe}$ and $\omega_{\rm pm}$ are the electric and magnetic plasma frequencies; $\gamma_{\rm e}$ and $\gamma_{\rm m}$ are the electric and magnetic loss or gain coefficients, respectively. It is noted that in $\mathcal{PT}$-symmetric MMs, the EM parameters $\varepsilon_{\rm r}$ and $\mu_{\rm r}$ are functions of frequency ϖ and space coordinate x; moreover, they follow the $\mathcal{PT}$-symmetric rules, i.e., $\varepsilon_{\rm r}(\varpi, x) = \varepsilon_{\rm r}^*(\varpi, -x)$ and $\mu_{\rm r}(\varpi, x) = \mu_{\rm r}^*(\varpi, -x)$ [38,51]. Thus, Eq. (8) can be used to investigate the transmission of EM waves in $\mathcal{PT}$-symmetric MMs. Considering the transmission properties of the EM waves in non-$\mathcal{PT}$-symmetric MMs can be characterized by the frequency-dependent permittivity and permeability [45,46], which are significantly different from those in conventional materials, it is necessary to explore the existence and controllable transmission of solitons in $\mathcal{PT}$-symmetric MMs.

For convenience, we firstly normalize Eq. (8) by $Z = z/L_D$, $X = x/W$, $U = \sqrt{\gamma L_D}E_x$, where $L_D = |\beta|W^2$ is the diffraction length, $\beta = nk_0$ is the wave number, and W is the beam width. The normalized equation in dimensionless units can be written as

$$i\frac{\partial U}{\partial Z} = -\frac{1}{2}\text{sgn}(n)\frac{\partial^2 U}{\partial X^2} + \text{sgn}(n)p\frac{\partial^4 U}{\partial X^4} - \delta(n + i2\alpha)U - (\rho + i\sigma)|U|^2U. \tag{9}$$

Here $\text{sgn}(n) = \pm 1$ represents the positive or negative refractive index, $p = 1/(8|\beta|L_D)$ stands for the FOD, $\delta = k_0L_D/2$ is related to the linear potential, and $\rho = \text{sgn}(\chi_{\rm p})(1 + \frac{\chi_{\rm m}}{\chi_{\rm p}\eta_r^2\eta_{\rm rr}^2})$ and $\sigma = \text{sgn}(\chi_{\rm p})(\bar{\mu} + \frac{\bar{\varepsilon}\chi_{\rm m}}{\chi_{\rm p}\eta_r^2\eta_{\rm rr}^2})$ denote cubic nonlinearity and nonlinear loss or gain. It can be deduced from Eq. (9) that in $\mathcal{PT}$-symmetric MMs, the EM wave experiences normal SOD and anomalous FOD in the negative index region (NIR); oppositely, it experiences anomalous SOD and normal FOD in the positive index region (PIR). Also, it is noted that the nonlinear loss or gain σ is related to $\bar{\varepsilon}$ and $\bar{\mu}$, which means that the linear loss of the MMs plays an important role in the nonlinearity effects [50]. In this paper, only the nonlinear polarization is considered, i.e., $\chi_{\rm m} = 0$, the nonlinear coefficients ρ and σ can be simplified as $\rho = \text{sgn}(\chi_{\rm p})$, $\sigma = \text{sgn}(\chi_{\rm p})\bar{\mu}$. According to the above expressions of parameters, $\bar{\mu}$ is negligible when $\gamma_{\rm m} = 5 \times 10^{-4}$ [46,50], resulting in a negligible absorption σ. Therefore, in the subsequent analysis, we take $\gamma_0 = \gamma_{\rm e}$, $\rho = \text{sgn}(\chi_{\rm p})$, and $\sigma = 0$. In addition, the FOD effect is essential for the transmission of ultrashort EM waves; however, it is much weaker than the SOD for general EM waves. Therefore, here we omit the FOD and only consider the SOD in the transmission model for the EM waves in $\mathcal{PT}$-symmetric MMs, which can be reduced to the following form,

$$i\frac{\partial U}{\partial Z} + \frac{1}{2}\text{sgn}(n)\frac{\partial^2 U}{\partial X^2} + V(\varpi, X)U + \text{sgn}(\chi_{\rm p})|U|^2U = 0, \tag{10}$$

where $V(\varpi, X) = \delta n(\varpi, X) + i2\delta\alpha(\varpi, X)$. It should be pointed out that Eq. (10) is in the same form as the one in

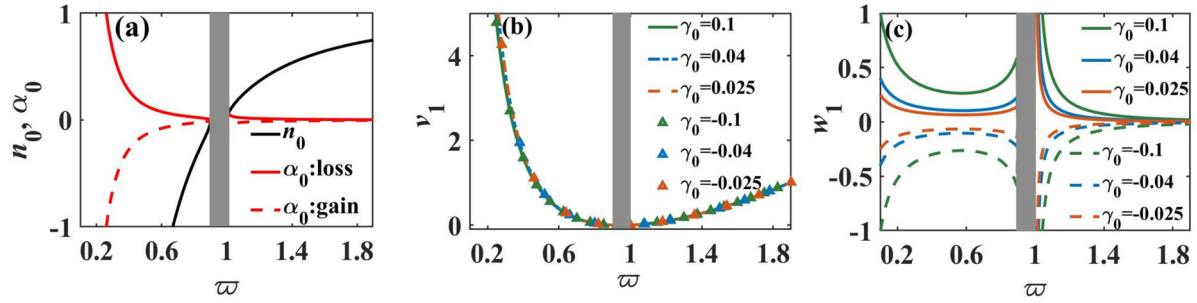

FIG. 1. (a) Background refractive index n_0, loss: gain α_0, (b) depth v_1, and (c) imaginary part w_1 of the $\mathcal{PT}$ potential for $\varpi_p = 0.9$, in which the gray areas denote the stop bands.

the optical lattice [20]; however, there exist fundamental differences between them. The coefficients of the derived model (10) are the function of frequency and refraction index as a result of the strong dispersive permittivity, permeability, and refractive index of MMs, featuring the controllable transmission of EM waves in nonlinear MMs. Moreover, the MMs can work in positive or negative index regimes with different diffraction, which will bring about some results disclosed in the subsequent section. Assuming $\mathcal{PT}$-symmetric MMs have periodically modulated refractive index $\mathrm{n} = n_0(\varpi)\cos^2(X)$ and loss or gain $\alpha = \alpha_0(\varpi)\sin(2X)$ [52], where n_0 and α_0 are the respective background refractive index and loss or gain, thus the linear potential will take the form of $V(\varpi, X) = v_1[\mathrm{sgn}(n_0)\cos^2(X) + iw_1\sin(2X)]$; $v_1 = \delta|n_0(\varpi)|$ and $w_1 = \frac{2\alpha_0(\varpi)}{|n_0(\varpi)|}$ denote the depth and imaginary part of the $\mathcal{PT}$ potential, respectively. Such $\mathcal{PT}$-symmetric potential in MMs can be experimentally realized on a Si-based optical platform with periodically arranged sinusoidal shaped combo structures [52], where the real and imaginary part modulations are implemented by elaborately designed Si and Ge or Cr structures, respectively.

According to the Drude model, the refractive index region of MMs can be divided into the NIR ($\varpi < \min\{\varpi_p, 1\}$), the PIR ($\varpi > \max\{\varpi_p, 1\}$), and the stop band region ($\min\{\varpi_p, 1\} < \varpi < \max\{\varpi_p, 1\}$). Without loss of generality, we set $\varpi_p = 0.9$ throughout this paper [42,46]. Figure 1 presents the variation of the parameters related to the $\mathcal{PT}$ potential with normalized frequency ϖ. From Fig. 1(a), it can be seen that the background refractive index n_0 monotonically changes with ϖ and the loss or gain parameter α_0 varies dramatically with the increase of ϖ in the NIR ($\varpi < 0.9$) and varies very slowly over the PIR ($\varpi > 1$). From Figs. 1(b) and 1(c), it can be found that γ_0 has little effect on the depth v_1 of the $\mathcal{PT}$ potential, while it strongly affects the imaginary part w_1 of the $\mathcal{PT}$ potential. It is worth noting that the variations of v_1 and w_1 with ϖ and γ_0 are much larger in the NIR than those in the PIR, which implies that one can easily regulate the $\mathcal{PT}$-symmetric potential in the NIR by choosing the frequency of the EM waves and material loss or gain. Figure 2 shows the profiles of $\mathcal{PT}$-symmetric potentials for different ϖ and γ_0. It can be seen from Figs. 2(a)–2(c) that depending on the values of ϖ and γ_0, the $\mathcal{PT}$ potentials can behave as a well or a barrier with different depths when the MMs operate in the NIR or PIR. The tunable $\mathcal{PT}$ potentials can give rise to abundant band structures, which will affect the controllable transmission characteristics of solitons in the $\mathcal{PT}$-symmetric MMs.

III. SOLITONS IN $\mathcal{PT}$-SYMMETRIC MMs

A. Tunable band structure and eigenvalue problem

Assuming the stationary solution of Eq. (10) possesses the form of $U(X, Z) = \psi(X)\exp(i\mu Z)$, where μ is the propagation constant and $\psi(X)$ is a complex function, substituting it into Eq. (10) will yield the following differential equation:

$$-\mu\psi + \frac{1}{2}\mathrm{sgn}(n)\frac{\partial^2\psi}{\partial X^2} + V(\varpi, X)\psi + \mathrm{sgn}(\chi_p)|\psi|^2\psi = 0. \tag{11}$$

Here the $\mathcal{PT}$ potentials $V(\varpi, X)$ are a function of both frequency ϖ and space coordinate X; the coefficients of SOD and cubic nonlinearity are related to the sign of the refractive index n and the nonlinear susceptibility χ_p. It is noted that Eq. (11) can be used to study the solitons in the NIR with normal SOD and in the PIR with anomalous SOD for defocusing ($\chi_p < 0$) or focusing ($\chi_p > 0$) nonlinearity. For a given ϖ, the soliton of Eq. (11) can be numerically solved by the modified squared operator iteration method [53,54], and the soliton power is defined as $P = \int_{-\infty}^{+\infty}|\psi|^2 dX$.

Due to the periodicity of $\mathcal{PT}$-symmetric potentials, the existence of solitons is determined by the band structure [55]. According to the Bloch theorem, the linear version of Eq. (11), $-\mu\psi + \frac{1}{2}\mathrm{sgn}(n)\frac{\partial^2\psi}{\partial X^2} + V(X)\psi = 0$, possesses Floquet-Bloch modes whose folding in momentum k forms Bloch bands [56]. Figure 3 shows the first three Bloch bands in the NIR ($\varpi < 0.9$) and PIR ($\varpi > 1$) when γ_0=0.1. It is observed from Figs. 3(a) and 3(b) that the band structure in the NIR has a wider tunable range by changing ϖ than that in the PIR, which is consistent with the characteristics of v_1 and w_1 shown in Figs. 1(b) and 1(c). Combining Fig. 1(c) with Fig. 3(a), there exists a critical frequency $\varpi_{th} = 0.21$ in the NIR corresponding to the phase transition point $w_1 = 0.5$, where the first and second Bloch bands begin to merge together. Figures 3(c)–3(e) present the band structures in the NIR for the cases of the broken $\mathcal{PT}$ symmetry ($\varpi = 0.2$), the phase transition point ($\varpi_{th} = 0.21$), and the unbroken $\mathcal{PT}$ symmetry ($\varpi = 0.31$), respectively. As the band structure depends on the sign of the refractive index, it is easy to deduce from the above linear version of Eq. (11) that the PIR band

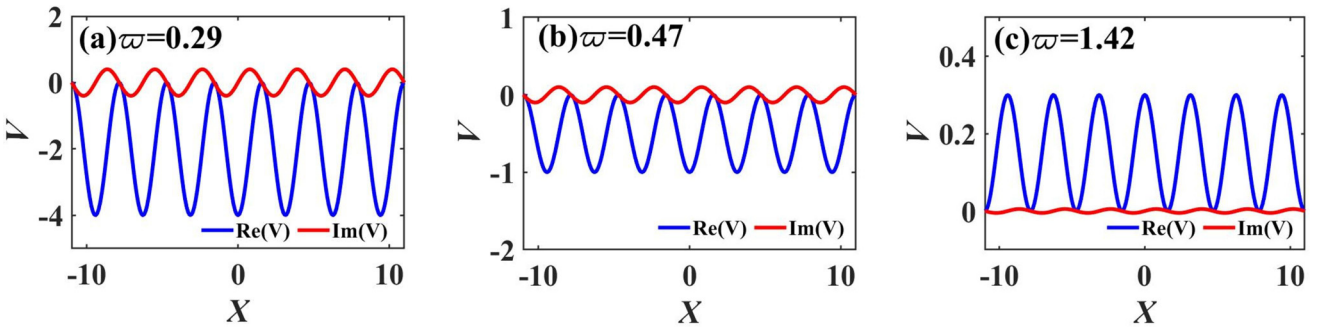

FIG. 2. Profiles of $\mathcal{PT}$-symmetric potential with different parameters. (a) $\varpi = 0.29$, $\gamma_0 = 0.025$, corresponding to $v_1 = 4$, $w_1 = 0.1$; (b) $\varpi = 0.47$, $\gamma_0 = 0.04$, corresponding to $v_1 = 1$, $w_1 = 0.1$, and (c) $\varpi = 1.42$, $\gamma_0 = 0.025$, corresponding to $v_1 = 0.3$, $w_1 = 0.02$, respectively.

structure is qualitatively upside down compared to the NIR; hence Fig. 3(f) only shows the band structure for the unbroken case ($\varpi = 1.77$) in the PIR. It should be noted that the $\mathcal{PT}$ potential parameter w_1 is tunable in $\mathcal{PT}$-symmetric MMs [see Fig. 1(c)]; one can regulate w_1 to maintain the unbroken $\mathcal{PT}$ symmetry in the PIR and NIR by changing the frequency of the EM waves. Therefore, in the subsequent analysis we focus on the case of unbroken $\mathcal{PT}$ symmetry.

To analyze the linear stability of solitons, we add the small perturbations $g(X)$ and $t(X)$ to the stationary solution:

$$U(X,Z) = [\psi(X) + g(X)\exp(\lambda Z) + t^*(X)\exp(\lambda^* Z)]\exp(i\mu Z). \tag{12}$$

Here, $g(X)$, $t(X) \ll \psi(X)$; "*" represents the complex conjugation. Substituting Eq. (12) into Eq. (10) and linearizing it around ψ yields an eigenvalue problem:

$$\lambda\begin{pmatrix} g \\ t \end{pmatrix} = i\begin{pmatrix} D + C_1 & C_2 \\ -C_2^* & -(D + C_1^*) \end{pmatrix}\begin{pmatrix} g \\ t \end{pmatrix},$$

$$D = \frac{1}{2}\mathrm{sgn}(n)\frac{\partial^2}{\partial x^2},$$

$$C_1 = -\mu + V + 2\mathrm{sgn}(\chi_p)|\psi|^2,$$

$$C_2 = \mathrm{sgn}(\chi_p)\psi^2. \tag{13}$$

The perturbation eigenvalue λ is numerically calculated by the Fourier collocation method [53], which can be used to predict the stability of solitons. If the real part of λ is equal to zero, i.e., $\mathrm{Re}(\lambda) = 0$, the soliton will propagate stably. It is noted that Eq. (13) is closely related to the signs of n and χ_p; therefore, the eigenvalue problem in Eq. (13) can be divided into two cases: (i) in the NIR $\mathrm{sgn}(n) = -1$, $\mathrm{sgn}(\chi_p) = \pm 1$; (ii) in the PIR $\mathrm{sgn}(n) = 1$, $\mathrm{sgn}(\chi_p) = \pm 1$. The existence and stability of solitons in these two cases will be discussed in detail.

B. Existence and stability of solitons in $\mathcal{PT}$-symmetric MMs

Based on the band structure and the linear-stability analysis, we consider the existence and stability of fundamental and dipole gap solitons. Figure 4 plots the variations of the soliton power P with the propagation constant μ for typical frequencies of incident waves in the NIR ($\varpi = 0.29,\ 0.47$) and PIR

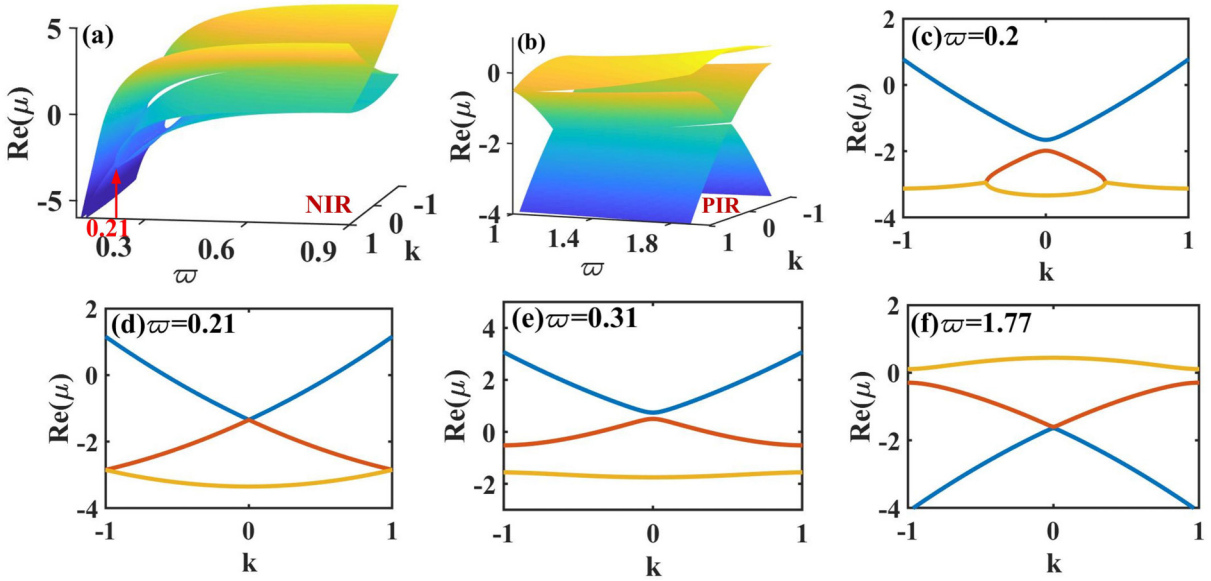

FIG. 3. Band structures in the (a) NIR and (b) PIR of $\mathcal{PT}$-symmetric MMs, (c) $\varpi = 0.2$ ($v_1 = 7.31$, $w_1 = 0.52$); (d) $\varpi = 0.21$ ($v_1 = 6.69$, $w_1 = 0.5$); (e) $\varpi = 0.31$ ($v_1 = 3.01$, $w_1 = 0.36$); (f) $\varpi = 1.77$ ($v_1 = 0.79$, $w_1 = 0.02$); the other parameters are $\gamma_0 = 0.1$, $\varpi_p = 0.9$.

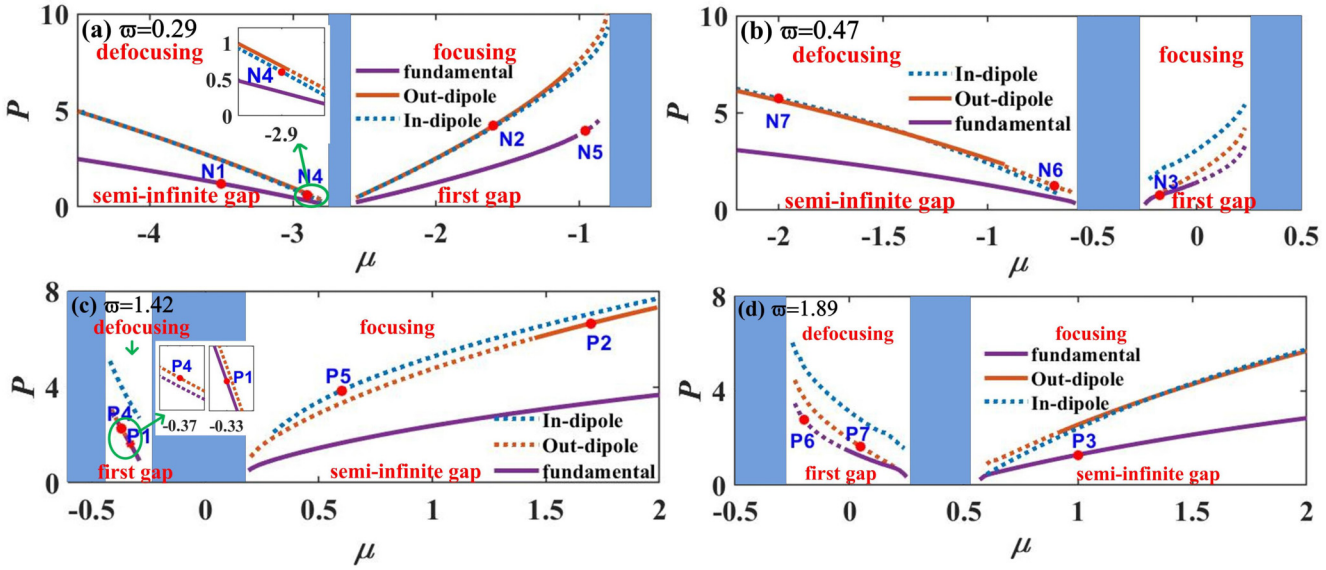

FIG. 4. Power P versus the propagation constant μ in the NIR and PIR of $\mathcal{PT}$-symmetric MMs. (a) $\varpi = 0.29$ ($v_1 = 4$, $w_1 = 0.1$); (b) $\varpi = 0.47$ ($v_1 = 1$, $w_1 = 0.1$); (c) $\varpi = 1.42$ ($v_1 = 0.3$, $w_1 = 0.02$); (d) $\varpi = 1.89$ ($v_1 = 1$, $w_1 = 0.01$).The blue areas correspond to the Bloch band. The soliton profiles at the points marked by N1–N7 (in the NIR) and P1–P7 (in the PIR) will be displayed in Figs. 5 and 6, respectively.

($\varpi = 1.42,\ 1.89$) of MMs, where the solid and dotted lines correspond to the stable and unstable solitons, respectively.

In the NIR shown in Figs. 4(a) and 4(b), it is found that the solitons can exist in the semi-infinite gap for defocusing nonlinearity and in the first gap for focusing nonlinearity. Specifically, in the semi-infinite gap, the fundamental solitons are stable while the in-dipoles are unstable over the entire existence range, but the out-dipoles can stay stable above the critical power $P_{\rm cr} = 0.67$ for $\varpi = 0.29$ ($v_1 = 4$, $w_1 = 0.1$) and $P_{\rm cr} = 2.35$ for $\varpi = 0.47$ ($v_1 = 1$, $w_1 = 0.1$), respectively. The instability of the in (out)-dipoles is caused by the mutual attraction (repulsion) between the soliton components. In the first gap, the in-dipoles for $\varpi = 0.29$ and $\varpi = 0.47$ are unstable over the whole gap; the out-dipoles for $\varpi = 0.29$ are stable below the critical power $P_{\rm cr} = 7.01$, while they are unstable for $\varpi = 0.47$ over the whole gap, which results from the narrower gap for a shallower $\mathcal{PT}$-symmetric potential ($v_1 = 1$ at $\varpi = 0.47$). However, the fundamental solitons are stable below the critical power $P_{cr} = 3.59$ for $\varpi = 0.29$ and $P_{cr} = 1.39$ for $\varpi = 0.47$, respectively. Comparing the results for $\varpi = 0.29$ and $\varpi = 0.47$, it can be concluded that the shallower potential can expand the instability range of the solitons in both the semi-infinite gap and the first gap, but suppress the existence range in the first gap.

In the PIR shown in Figs. 4(c) and 4(d), it is observed that the solitons can exist in the first gap for defocusing nonlinearity and in the semi-infinite gap for focusing nonlinearity, which is different from the case in the NIR. This is because the sign of the refractive index directly affects the diffraction effect in Eq. (11). Obviously, the first gap for $\varpi = 1.42$ ($v_1 = 0.3$, $w_1 = 0.02$) is much narrower than that for $\varpi = 1.89$ ($v_1 = 1$, $w_1 = 0.01$). In the first gap, the fundamental solitons are stable below the critical power $P_{\rm cr} = 1.78$ for $\varpi = 1.42$ and $P_{\rm cr} = 1.48$ for $\varpi = 1.89$, respectively. However, the dipole solitons, regardless of out-dipoles or in-dipoles, are completely unstable, which stems from the weakened localization for the shallower $\mathcal{PT}$ potentials for $\varpi = 1.42$ and $\varpi = 1.89$, respectively. This is quite different from the instability of the dipole solitons in a deeper potential ($v_1 = 4$ for $\varpi = 0.29$). In the semi-infinite gap, the fundamental solitons are completely stable and the in-dipoles are unstable over the whole existence range for both $\varpi = 1.42$ and $\varpi = 1.89$, while the out-dipoles are stable above the critical power $P_{\rm cr} = 6.03$ for $\varpi = 1.42$ and $P_{\rm cr} = 2.30$ for $\varpi = 1.89$, respectively. The results presented here imply that the existence and stability of the fundamental, out-dipole, and in-dipole gap solitons can be controlled flexibly by changing the frequency of incident waves.

Furthermore, the stability of the fundamental and dipole solitons is verified by direct simulations under 5% random noise perturbations. The linear spectra, profiles, and evolutions of the stable $\mathcal{PT}$-symmetric solitons at the points N1–N3 in the NIR and P1–P3 in the PIR (marked in Fig. 4) are presented in Fig. 5, where the blue and red lines in Figs. 5(a1)–5(f1) are for the real and imaginary parts of the solitons. It can be clearly seen that the fundamental soliton and the out-dipole solitons at the points N1–N3 and P1–P3 can propagate stably against perturbations, as shown in Figs. 5(a3)–5(f3), which are consistent with the linear spectra with pure imaginary values [see Figs. 5(a2)–5(f2)]. The unstable solitons at the points N4–N7 and P4–P7 marked in Fig. 4 are presented in Fig. 6, exhibiting various unstable behaviors. Comparing the profiles of solitons in Fig. 6(g1) with Figs. 6(h1) and 5(d1) with Fig. 6(e1), it is found that the localization of solitons in the same existence region remains consistent, which directly stems from the formation conditions of solitons and the values of $\mathcal{PT}$ potential parameters. Moreover, the fundamental solitons start diffraction after stable propagation over a longer distance, as shown in Figs. 6(b3) and 6(g3), while the dipole solitons evolve asymmetrically [see Figs. 6(a3), 6(c3), 6(d3), 6(f3), and 6(h3)], which originates from the interaction between the components of the solitons. The instability of

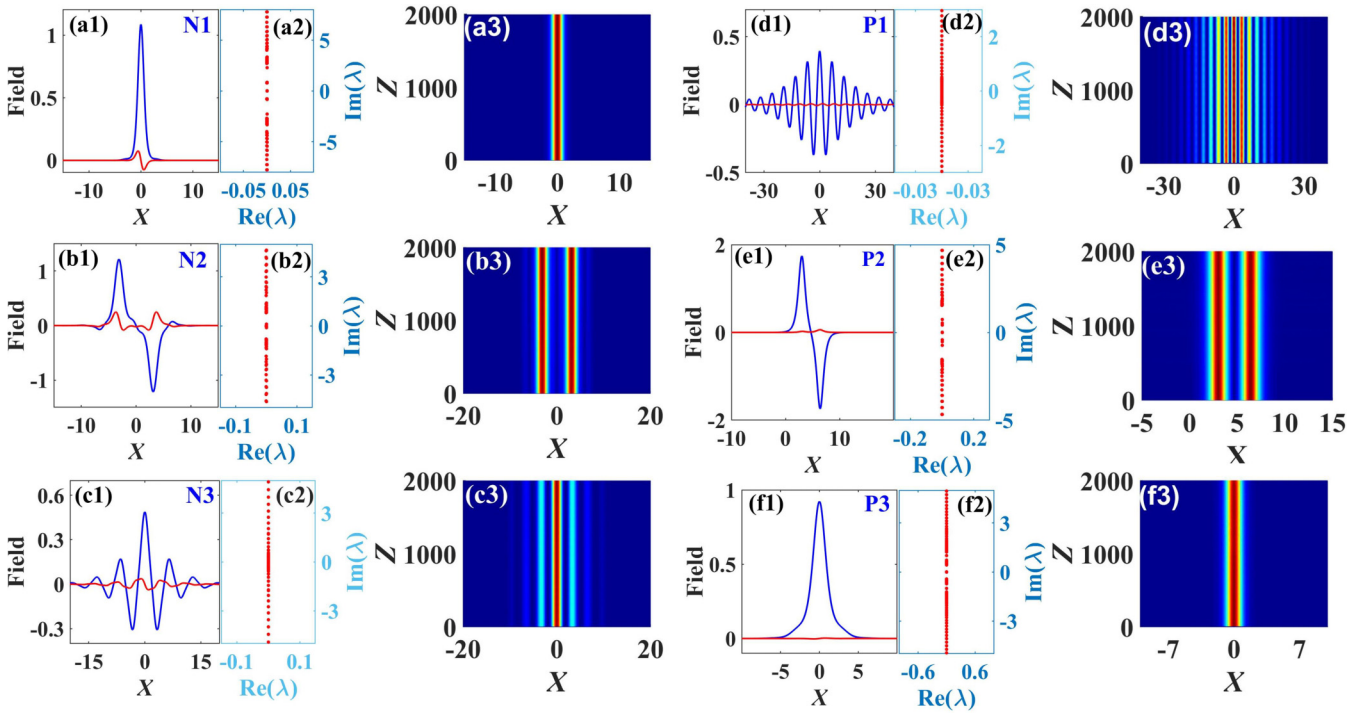

FIG. 5. Profiles, linear spectra, and nonlinear evolutions of the stable solitons at the points (a) N1: $\mu = -3.5$; (b) N2: $\mu = -1.6$; (c) N3: $\mu = -0.18$; (d) P1: $\mu = -0.33$; (e) P2: $\mu = 1.7$; and (f) P3: $\mu = 1$, which are marked in Fig. 4.

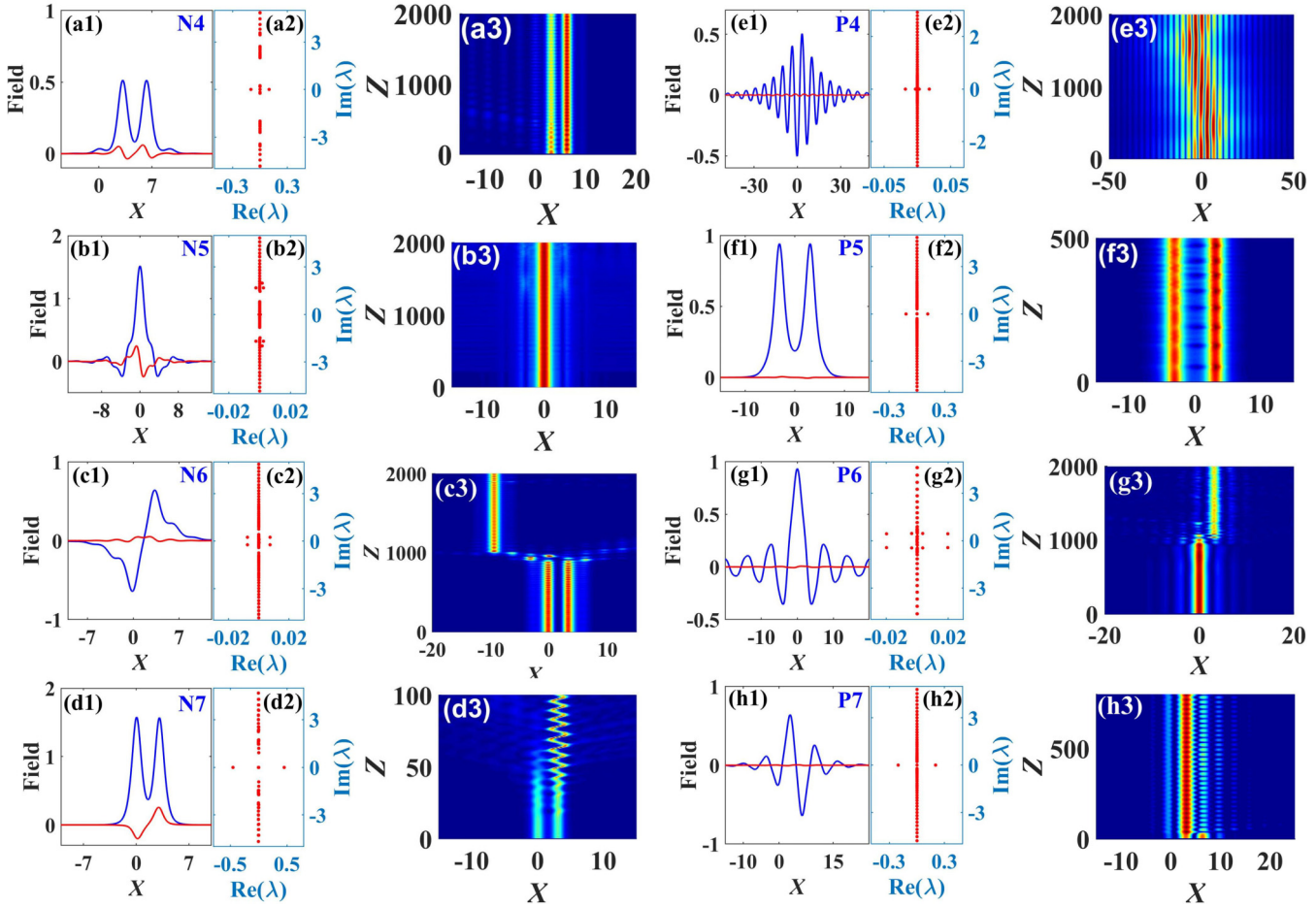

FIG. 6. Profiles, linear spectra, and nonlinear evolutions of the unstable solitons at the points (a) N4: $\mu = -2.9$; (b) N5: $\mu = -0.96$; (c) N6: $\mu = -0.68$; (d) N7: $\mu = -2$; (e) P4: $\mu = -0.37$; (f) P5: $\mu = 0.6$; (g) P6: $\mu = -0.2$; and (h) P7: $\mu = 0.05$, which are marked in Fig. 4.

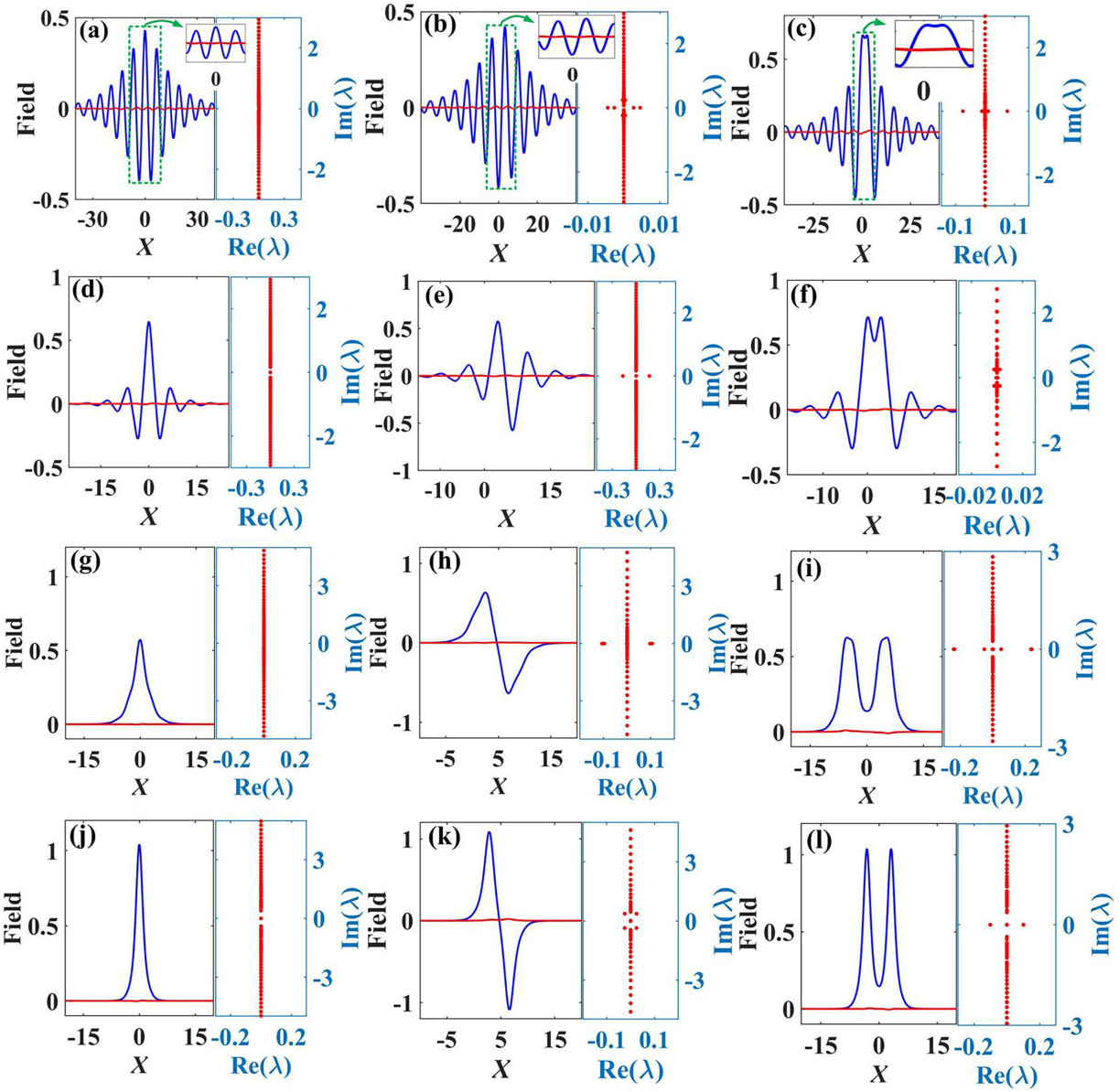

FIG. 7. Profiles and linear spectra of fundamental, out-dipole and in-dipole solitons. (a)–(c) $\mu = -0.34$ at $\varpi = 1.42$ ($v_1 = 0.3$, $w_1 = 0.02$) and (d)–(f) $\mu = 0.1$ at $\varpi = 1.89$ ($v_1 = 1$, $w_1 = 0.01$) for defocusing nonlinearity; (g)–(i) $\mu = 0.4$ ($P = 0.95, 2.20, 3.19$) and (j)–(l) $\mu = 0.7$ ($P = 1.86, 3.73, 3.75$) for focusing nonlinearity at $\varpi = 1.42$, respectively.

solitons at the points N4–N7 and P4–P7 is consistent with the pairwise appearance of pure real or complex perturbed eigenvalues in the linear spectra in Figs. 6(a2)–6(h2). The stability analysis of solitons lays the foundation for the investigation of nonlinear EM waves in $\mathcal{PT}$-symmetric MMs, which can be used for signal encryption and the fabrication of optical devices.

C. Enhanced localization of $\mathcal{PT}$-symmetric solitons

As demonstrated in Figs. 5 and 6, the localization and stability of the solitons highly depend on the parameters of the $\mathcal{PT}$ potential and the nonlinearity effect, exhibiting diverse characteristics. In order to further elucidate the intrinsic connection, the profiles and linear spectra of fundamental and dipole solitons under different formation conditions are presented in Fig. 7. For a shallower $\mathcal{PT}$ potential ($v_1 = 0.3$), weak localization occurs for defocusing nonlinearity. The real part of the solitons features decaying oscillatory behavior with strong side lobes [Figs. 7(a)–7(c)]; in particular, from the insets in Figs. 7(a)–7(c), it is obviously found that the fundamental soliton has maximum peaks only at $x = 0$; the two main peaks of the out-dipole soliton are odd symmetric about the center of the soliton, while the two main peaks of the in-dipole soliton are even symmetric with a small separation. This mainly originates from the excitation and interference of multiple modes. On the other hand, increasing the depth of the $\mathcal{PT}$ potential ($v_1 = 1$) can promote the localization of solitons, which can be found by comparing the profiles of solitons in Figs. 7(d)–7(f) with Figs. 7(a)–7(c). Furthermore, the localization of solitons for shallower potentials ($v_1 = 0.3$) are investigated in focusing nonlinearity, as

shown in Figs.7(g)–7(l). It is found that the localization of the solitons can be enhanced in the focusing nonlinear MMs; the side lobes of solitons disappear completely. Moreover, by comparing the profiles and linear spectra of solitons in Figs. 7(g)–7(i) corresponding to the power $P = 0.95$, 2.20, 3.19, and Figs. 7(j)–7(l) corresponding to the power $P = 1.86$, 3.73, 3.75 under focusing nonlinearity at $\varpi = 1.42$, it is obviously observed that the localization of solitons is further enhanced with the increase of power P. Therefore, in $\mathcal{PT}$-symmetric MMs, deeper potentials can overcome the weak localization for defocusing nonlinearity, while the focusing nonlinearity can enhance the localization for shallower potentials, and the power has a distinct effect on the localization of solitons. For those cases, the enhanced localization can be realized by choosing a suitable frequency of incident EM waves.

IV. CONCLUSION AND DISCUSSION

In summary, starting from Maxwell equations and the Drude model, we have established a general theoretical model that can be used to describe the transmission of EM waves in nonlinear $\mathcal{PT}$-symmetric MMs, where the $\mathcal{PT}$ potential is not only a function of space coordinators, but also a function of frequency. Thus, the $\mathcal{PT}$-symmetric MMs have abundant tunable linear band structure and a nonlinear eigenvalue problem in negative and positive index regions, and there is a larger tunable range in NIR than in PIR, which results in the frequency-dependent gap range and existence region of solitons being quite different from those in an optical lattice [20]. Based on the established transmission model, we have predicted the existence ranges, stability, and localization of fundamental, out-dipole, and in-dipole solitons with different incident frequencies. It is found that in the NIR, the $\mathcal{PT}$-symmetric solitons exist in the semi-infinite (first) gap for defocusing (focusing) nonlinearity; oppositely in the PIR, the solitons exist in the first (semi-infinite) gap for defocusing (focusing) nonlinearity. Moreover, the stability of the solitons depends on the existence ranges and the $\mathcal{PT}$ potential parameters. Specifically, the fundamental soliton is stable in the semi-infinite gap, while is stable below a lower critical power in the first gap; however, the in-dipole solitons are completely unstable in their existence ranges; the out-dipole solitons are stable in the semi-infinite gap above the critical power, while they are stable for deeper potentials below the critical power and unstable for shallower potentials in the first gap. Furthermore, we reveal deeper potentials can overcome the weak localization from defocusing nonlinearity, and focusing nonlinearity can enhance the localization even for shallower potentials, and the power also can influence the localization of solitons. Our research may profoundly enrich the transmission theory of solitons in nonlinear optics, and provides fertile ground for the research of tunable solitons and the flexible manipulation of EM waves.

It should be pointed out that the preceding analysis focuses on bright fundamental, dipole gap solitons in the case including only SOD in $\mathcal{PT}$-symmetric MMs. In fact, for the transmission of ultrashort EM waves in $\mathcal{PT}$-symmetric MMs, the FOD effect in the model equation (9) should be considered, which will be discussed in the future. In addition, dark solitons and vortices will also be explored in $\mathcal{PT}$-symmetric MMs with the FOD and nonlinear absorption. Most recently, the spontaneous symmetry breaking in $\mathcal{PT}$-symmetric MMs is under consideration. Many characteristics and manipulation of EM waves in $\mathcal{PT}$-symmetric MMs will be discovered in the future.

ACKNOWLEDGMENTS

The authors thank Prof. P. G. Kevrekidis from the University of Massachusetts for his insights and suggestions, which have substantially improved our paper. This work was supported by the National Natural Science Foundation of China (Grants No. 61775126 and No. 62305199) and the Natural Science Foundation of Shanxi Province (GrantNo. 202203021221016).

[1] C. M. Bender and S. Boettcher, Real spectra in non-Hermitian Hamiltonians having $\mathcal{PT}$ symmetry, Phys. Rev. Lett. **80**, 5243 (1998).

[2] C. M. Bender, D. C. Brody, and H. F. Jones, Complex extension of quantum mechanics, Phys. Rev. Lett. **89**, 270401 (2002).

[3] A. Regensburger, C. Bersch, M.-A. Miri, G. Onishchukov, D. N. Christodoulides, and U. Peschel, Parity-time synthetic photonic lattices, Nature (London) **488**, 167 (2012).

[4] G. M. Li, A. Li, S. J. Su, Y. Zhao, K. Y. Huang, G. P. Zhou, L. Xue, and S. L. Xu, Vector spatiotemporal solitons in cold atomic gases with linear and nonlinear $\mathcal{PT}$ symmetric potentials, Opt. Express **29**, 14016 (2021).

[5] Y. M. Xue, C. Hang, Y. H. He, Z. Y. Bai, Y. C. Jiao, G. X. Huang, J. M. Zhao, and S. T. Jia, Experimental observation of partial parity-time symmetry and its phase transition with a laser-driven cesium atomic gas, Phys. Rev. A **105**, 053516 (2022).

[6] X. Zhu, H. Ramezani, C. Shi, J. Zhu, and X. Zhang, $\mathcal{PT}$-symmetric acoustics, Phys. Rev. X **4**, 031042 (2014).

[7] M. Küß, M. Hassan, Y. Kunz, A. Hörner, M. Weiler, and M. Albrecht, Nonreciprocal transmission of magnetoacoustic waves in compensated synthetic antiferromagnets, Phys. Rev. B **107**, 214412 (2023).

[8] C. M. Bender, B. K. Berntson, D. Parker, and E. Samuel, Observation of $\mathcal{PT}$ phase transition in a simple mechanical system, Am. J. Phys. **81**, 173 (2013).

[9] J. Schindler, A. Li, M. C. Zheng, F. M. Ellis, and T. Kottos, Experimental study of active LRC circuits with $\mathcal{PT}$ symmetries, Phys. Rev. A **84**, 040101(R) (2011).

[10] V. V. Konotop, J. K. Yang, and D. A. Zezyulin, Nonlinear waves in $\mathcal{PT}$-symmetric systems, Rev. Mod. Phys. **88**, 035002 (2016).

[11] S. V. Suchkov, A. A. Sukhorukov, J. H. Huang, S. V. Dmitriev, C. H. Lee, and Y. S. Kivshar, Nonlinear switching and solitons in $\mathcal{PT}$-symmetric photonic systems, Laser Photonics Rev. **10**, 177 (2016).

[12] S. Longhi, Quantum-optical analogies using photonic structures, Laser Photonics Rev. **3**, 243 (2009).

[13] Ş. K. Özdemir, S. Rotter, F. Nori, and L. Yang, Parity-time symmetry and exceptional points in photonics, Nat. Mater. **18**, 783 (2019).

[14] K. G. Makris, R. El-Ganainy, D. N. Christodoulides, and Z. H. Musslimani, Beam dynamics in $\mathcal{PT}$ symmetric optical lattices, Phys. Rev. Lett. **100**, 103904 (2008).

[15] L. W. Zeng, J. C. Shi, X. W. Lu, Y. Cai, Q. F. Zhu, H. Y. Chen, H. Long, and J. Z. Li, Stable and oscillating solitons of $\mathcal{PT}$-symmetric couplers with gain and loss in fractional dimension, Nonlinear Dyn. **103**, 1831 (2021).

[16] W. H. Wang, Y. F. Zhang, B. Li, J. Wang, J. G. Ma, P. Yuan, D. F. Zhang, H. Zhang, and L. J. Qian, Generation of an ultrashort pulse train through ultrafast parity-time symmetry switching, Opt. Express **31**, 19523 (2023).

[17] Y. L. Song, S. L. Ke, Y. L. Chen, and M. F. Wang, Mode-locking in anti-$\mathcal{PT}$ symmetric frequency lattices, Appl. Phys. Lett. **122**, 151106 (2023).

[18] A. Guo, G. J. Salamo, D. Duchesne, R. Morandotti, M. Volatier-Ravat, V. Aimez, G. A. Siviloglou, and D. N. Christodoulides, Observation of $\mathcal{PT}$-symmetry breaking in complex optical potentials, Phys. Rev. Lett. **103**, 093902 (2009).

[19] M.-A. Miri, A. Regensburger, U. Peschel, and D. N. Christodoulides, Optical mesh lattices with $\mathcal{PT}$ symmetry, Phys. Rev. A **86**, 023807 (2012).

[20] S. Nixon, L. J. Ge, and J. K. Yang, Stability analysis for solitons in $\mathcal{PT}$-symmetric optical lattices, Phys. Rev. A **85**, 023822 (2012).

[21] Z. H. Musslimani, K. G. Makris, R. El-Ganainy, and D. N. Christodoulides, Optical solitons in $\mathcal{PT}$ periodic potentials, Phys. Rev. Lett. **100**, 030402 (2008).

[22] Y. Chen, Z. Y. Yan, and D. Mihalache, Soliton formation and stability under the interplay between parity-time-symmetric generalized Scarf-II potentials and Kerr nonlinearity, Phys. Rev. E **102**, 012216 (2020).

[23] X. Li, L. Wang, Z. J. Zhou, Y. Chen, and Z. Y. Yan, Stable dynamics and excitations of single- and double-hump solitons in the Kerr nonlinear media with $\mathcal{PT}$-symmetric HHG potentials, Nonlinear Dyn. **108**, 4045 (2022).

[24] M. Zhong, Y. Chen, Z. Y. Yan, and S. F. Tian, Formation, stability, and adiabatic excitation of peakons and double-hump solitons in parity-time-symmetric Dirac-δ(x)-Scarf-II optical potentials, Phys. Rev. E **105**, 014204 (2022).

[25] V. Achilleos, P. G. Kevrekidis, D. J. Frantzeskakis, and R. Carretero-González, Dark solitons and vortices in $\mathcal{PT}$-symmetric nonlinear media: From spontaneous symmetry breaking to nonlinear $\mathcal{PT}$ phase transitions, Phys. Rev. A **86**, 013808 (2012).

[26] J. K. Yang, Symmetry breaking of solitons in one-dimensional parity-time-symmetric optical potentials, Opt. Lett. **39**, 5547 (2014).

[27] P. F. Li, B. A. Malomed, and D. Mihalache, Symmetry-breaking bifurcations and ghost states in the fractional nonlinear Schrödinger equation with a $\mathcal{PT}$-symmetric potential, Opt. Lett. **46**, 3267 (2021).

[28] A. Sahoo, D. K. Mahato, A. Govindarajan, and A. K. Sarma, Bistable soliton switching dynamics in a $\mathcal{PT}$-symmetric coupler with saturable nonlinearity, Phys. Rev. A **105**, 063503 (2022).

[29] L. W. Zeng, M. R. Belić, D. Mihalache, J. C. Shi, J. W. Li, S. Q. Li, X. W. Lu, Y. Cai, and J. Z. Li, Families of gap solitons and their complexes in media with saturable nonlinearity and fractional diffraction, Nonlinear Dyn. **108**, 1671 (2022).

[30] V. M. Shalaev, Optical negative-index metamaterials, Nat. Photonics **1**, 41 (2007).

[31] D. R. Smith, J. B. Pendry, and M. C. K. Wiltshire, Metamaterials and negative refractive index, Science **305**, 788 (2004).

[32] S. Droulias, T. Koschny, M. Kafesaki, and C. M. Soukoulis, On loss compensation, amplification and lasing in metallic metamaterials, Nanomater. Nanotechnol. **9**, 1 (2019).

[33] A. D. Boardman, V. V. Grimalsky, Y. S. Kivshar, S. V. Koshevaya, M. Lapine, N. M. Litchinitser, V. N. Malnev, M. Noginov, Y. G. Rapoport, and V. M. Shalaev, Active and tunable metamaterials, Laser Photonics Rev. **5**, 287 (2011).

[34] J. Gear, F. Liu, S. T. Chu, S. Rotter, and J. Li, Parity-time symmetry from stacking purely dielectric and magnetic slabs, Phys. Rev. A **91**, 033825 (2015).

[35] T. Jiang, K. Chang, L. M. Si, L. X. Ran, and H. Xin, Active microwave negative-index metamaterial transmission line with gain, Phys. Rev. Lett. **107**, 205503 (2011).

[36] M. Sakhdari, M. Farhat, and P. Y. Chen, $\mathcal{PT}$-symmetric metasurfaces: Wave manipulation and sensing using singular points, New J. Phys. **19**, 065002 (2017).

[37] N. Lazarides and G. P. Tsironis, Gain-driven discrete breathers in $\mathcal{PT}$-symmetric nonlinear metamaterials, Phys. Rev. Lett. **110**, 053901 (2013).

[38] Y. Sun, W. Tan, H. Q. Li, J. Li, and H. Chen, Experimental demonstration of a coherent perfect absorber with $\mathcal{PT}$ phase transition, Phys. Rev. Lett. **112**, 143903 (2014).

[39] H. Alaeian and J. A. Dionne, Parity-time-symmetric plasmonic metamaterials, Phys. Rev. A **89**, 033829 (2014).

[40] S. Savoia, G. Castaldi, V. Galdi, A. Alù, and N. Engheta, $\mathcal{PT}$-symmetry-induced wave confinement and guiding in ε-near-zero metamaterials, Phys. Rev. B **91**, 115114 (2015).

[41] M. Nicolussi, J. A. Riley, and V. Pacheco-Peña, Unidirectional transparency in epsilon-near-zero based rectangular waveguides induced by parity-time symmetry, Appl. Phys. Lett. **119**, 263507 (2021).

[42] M. Scalora, M. S. Syrchin, N. Akozbek, E. Y. Poliakov, G. D'Aguanno, N. Mattiucci, M. J. Bloemer, and A. M. Zheltikov, Generalized nonlinear Schrödinger equation for dispersive susceptibility and permeability: Application to negative index materials, Phys. Rev. Lett. **95**, 013902 (2005).

[43] N. Lazarides and G. P. Tsironis, Coupled nonlinear Schrödinger field equations for electromagnetic wave propagation in nonlinear left-handed materials, Phys. Rev. E **71**, 036614 (2005).

[44] R. C. Yang and I. V. Shadrivov, Double-nonlinear metamaterials, Appl. Phys. Lett. **97**, 231114 (2010).

[45] S. C. Wen, Y. J. Xiang, X. Y. Dai, Z. X. Tang, W. H. Su, and D. Y. Fan, Theoretical models for ultrashort electromagnetic waves propagation in nonlinear metamaterials, Phys. Rev. A **75**, 033815 (2007).

[46] P. G. Li, R. C. Yang, and Z. Y. Xu, Gray solitary-waves solutions in nonlinear negative-index materials, Phys. Rev. E **82**, 046603 (2010).

[47] H. P. Zhu and H. Y. Chen, Parameter modulation of periodic waves and solitons in metamaterials with higher-order dispersive and nonlinear effects, Nonlinear Dyn. **104**, 1545 (2021).

[48] A. K. Shafeeque Ali, A. Govindarajan, and M. Lakshmanan, Stabilization of light bullets in nonlinear metamaterial waveguides, Phys. Rev. A **105**, 033516 (2022).

[49] A. D. Boardman, R. C. Mitchell-Thomas, N. J. King, and Y. G. Rapoport, Bright spatial solitons in controlled negative phase metamaterials, Opt. Commun. **283**, 1585 (2010).

[50] Y. J. Xiang, X. Y. Dai, S. C. Wen, and J. Guo, Nonlinear absorption due to linear loss and magnetic permeability in metamaterials, Phys. Rev. E **85**, 066604 (2012).

[51] D. V. Novitsky, A. S. Shalin, and A. Novitsky, Nonlocal homogenization of $\mathcal{PT}$-symmetric multilayered structures, Phys. Rev. A **99**, 043812 (2019).

[52] L. Feng, Y. L. Xu, W. S. Fegadolli, M. H. Lu, J. E. B. Oliveira, V. R. Almeida, Y. F. Chen, and A. Scherer, Experimental demonstration of a unidirectional reflectionless parity-time metamaterial at optical frequencies, Nat. Mater. **12**, 108 (2013).

[53] J. K. Yang and T. I. Lakoba, Universally-convergent squared-operator iteration methods for solitary waves in general nonlinear wave equations, Stud. Appl. Math. **118**, 153 (2007).

[54] J. K. Yang, *Nonlinear Waves in Integrable and Nonintegrable Systems* (SIAM, Philadelphia, 2010).

[55] C. M. Huang, C. Y. Li, and L. W. Dong, Stabilization of multipole-mode solitons in mixed linear-nonlinear lattices with a $\mathcal{PT}$ symmetry, Opt. Express **21**, 3917 (2013).

[56] L. W. Zeng and J. H. Zeng, One-dimensional gap solitons in quintic and cubic–quintic fractional nonlinear Schrödinger equations with a periodically modulated linear potential, Nonlinear Dyn. **98**, 985 (2019).